

# The gene repressor complex NuRD interacts with the histone variant H3.3 at promoters of active genes

Daniel C. Kraushaar,<sup>1,3,4</sup> Zuo Zhou Chen,<sup>2,3</sup> Qingsong Tang,<sup>1</sup> Kairong Cui,<sup>1</sup> Junfang Zhang,<sup>2</sup> and Keji Zhao<sup>1</sup>

<sup>1</sup>Systems Biology Center, National Heart, Lung, and Blood Institute, National Institutes of Health, Bethesda, Maryland 20892, USA;

<sup>2</sup>Key Laboratory of Exploration and Utilization of Aquatic Genetic Resources (Shanghai Ocean University), Ministry of Education; International Research Center for Marine Biosciences at Shanghai Ocean University, Ministry of Science and Technology; National Demonstration Center for Experimental Fisheries Science Education, Shanghai Ocean University, Shanghai 201306, China

The histone variant H3.3 is deposited across active genes, regulatory regions, and telomeres. It remains unclear how H3.3 interacts with chromatin modifying enzymes and thereby modulates gene activity. In this study, we performed a co-immunoprecipitation-mass spectrometry analysis of proteins associated with H3.3-containing nucleosomes and identified the nucleosome remodeling and deacetylase complex (NuRD) as a major H3.3-interactor. We show that the H3.3-NuRD interaction is dependent on the H3.3 lysine 4 residue and that NuRD binding occurs when lysine 4 is in its unmodified state. The majority of NuRD binding colocalizes with H3.3 and directly correlates with gene activity. H3.3 depletion led to reduced levels of NuRD at sites previously occupied by H3.3, as well as a global decrease in histone marks associated with gene activation. Our results demonstrate the importance of H3.3 in the maintenance of the cellular epigenetic landscape and reveal a highly prevalent interaction between the histone variant H3.3 and the multiprotein complex NuRD.

[Supplemental material is available for this article.]

The replacement of canonical histones with histone variants influences transcriptional gene regulation and epigenetic memory (Henikoff et al. 2004; Jin and Felsenfeld 2007; Jin et al. 2009; Elsaesser et al. 2010; Hu et al. 2013; Kraushaar and Zhao 2013). Unlike H3.1 and H3.2, which are expressed and incorporated into chromatin during S-phase only, H3.3 is deposited into chromatin independent of cell cycle stage (Ahmad and Henikoff 2002; Ray-Gallet et al. 2002). H3.3 differs from H3.1 and H3.2 in five and four amino acids, respectively, and it is these differences that convey specificity in binding to their respective chaperones (Tagami et al. 2004; Ray-Gallet et al. 2011). H3.3 is typically decorated with marks that are associated with gene activation, including H3K acetylation and H3K4 methylation, and less with marks related to gene silencing, such as H3K27 trimethylation and H3K9 methylation (Hake et al. 2006).

Chromatin components are dynamically exchanged during and outside of DNA replication. H3.3 is deposited by histone chaperones including HIRA and the ATRX/DAXX complex, which incorporate H3.3 at regulatory sites and heterochromatic sites, respectively (Goldberg et al. 2010; Lewis et al. 2010; Wong et al. 2010; Szenker et al. 2012). H3.3 incorporation is prevalent across active genes, as well as intergenic enhancers that are marked with H3K4 monomethylation and H3K27 acetylation (Goldberg et al. 2010; Kraushaar et al. 2013). Canonical H3 is replaced by H3.3 when gene transcription is triggered, with highest enrichment typically at the distal end of coding regions (Tamura et al. 2009). H3.3 becomes displaced and redeposited at different rates across the genome independent of replication. H3.3 turnover is

typically well correlated with total H3.3 enrichment, suggesting that H3.3 deposition is a feature of low nucleosome stability (Kraushaar et al. 2013; Ha et al. 2014). Indeed, biochemical experiments have shown that H3.3-containing nucleosomes are intrinsically unstable and sensitive to salt-dependent disruption (Jin and Felsenfeld 2007). Other data suggest an active role for proteasomal-dependent degradation in the eviction and turnover of H3.3 (Maze et al. 2015).

The nucleosome remodeling and deacetylase complex (NuRD) is a multiprotein complex exhibiting dual enzymatic functionality in the shape of ATP-dependent chromatin remodeling and histone deacetylation (Xue et al. 1998; Zhang et al. 1998). The NuRD complex plays a major role in transcriptional regulation and DNA damage repair (Torchy et al. 2015; Spruijt et al. 2016; Gong et al. 2017). The NuRD complex is composed of six subunits each with multiple isoforms: HDAC1/2, MTA1/2/3, RBBP4/7, GATAD2A/GATAD2B, MBD2/3, and CHD3/4 (Basta and Rauchman 2015; Torchy et al. 2015). Metastasis-associated protein1 (MTA1) and its homologs MTA2/3 serve as scaffold proteins for NuRD complex assembly and are up-regulated in various cancer tissues (Li and Kumar 2015). RBBP4 and RBBP7 are core components of NuRD but are present in other Class I HDAC corepressor complexes such as the Sin3A and PRC2 complexes (Torchy et al. 2015). The NuRD complex triggers gene repression through changes in histone modifications, most notably H3 lysine deacetylation and other chromatin remodeling activities such as histone variant deposition (Fujita et al. 2004; Kaji et al. 2006; Rais et al. 2013; Yamada et al. 2014; Kim et al. 2015; Yang et al. 2016).

<sup>3</sup>These authors contributed equally to this work.

<sup>4</sup>Present address: Genomic and RNA Profiling Core, Baylor College of Medicine, Houston, TX 77030, USA

Corresponding authors: jfzhang@shou.edu.cn, zhaok@nhlbi.nih.gov  
Article published online before print. Article, supplemental material, and publication date are at <http://www.genome.org/cgi/doi/10.1101/gr.236224.118>.

© 2018 Kraushaar et al. This article is distributed exclusively by Cold Spring Harbor Laboratory Press for the first six months after the full-issue publication date (see <http://genome.cshlp.org/site/misc/terms.xhtml>). After six months, it is available under a Creative Commons License (Attribution-NonCommercial 4.0 International), as described at <http://creativecommons.org/licenses/by-nc/4.0/>.

In this study, we immunoprecipitated chromatin-associated H3.3 followed by a mass spectrometry analysis to identify epigenetic regulators that interact with H3.3 and may shed further light on the functional role of this histone variant.

## Results

### H3.3 interacts with the nucleosome remodeling and deacetylase (NuRD) corepressor complex

In order to identify proteins that physically interact with H3.3 at the chromatin level, we expressed a HA/FLAG-tagged version of H3.3 under the control of doxycycline in NIH/3T3 mouse embryonic fibroblasts (MEFs), solubilized chromatin with MNase I, and immunoprecipitated H3.3-containing mononucleosomes with anti-FLAG antibody, followed by mass spectrometry (Fig. 1A). A Gene Ontology analysis revealed that protein partners of wild-type H3.3 are typically associated with chromosome and nucleosomal functions (Fig. 1B). To elucidate the importance of N-terminal lysine modifications for protein interactions with H3.3, we mutated lysine residues on amino acids 4, 9, 27, and 36 to arginine. Mutation of lysine residues to arginine prevented recognition of HA/FLAG-H3.3 by antibodies specific to H3 lysine methylation, when wild-type and mutant H3.3 proteins were expressed at comparable levels (Fig. 1C). Across HA/FLAG-H3.3 wild-type and HA/FLAG-H3.3 mutant samples, we identified a total of 114 proteins. Spectral counts provided a semiquantitative measurement of H3.3-protein interactions between wild-type H3.3 and mutant

H3.3 versions. Mutating lysine 4 had the largest effect, significantly reducing the spectral counts of 30 proteins. Mutating lysine 9 resulted in substantially lower spectral counts of 16 proteins, followed by relatively small effects of mutating lysine 27 and lysine 36 of HA/FLAG-H3.3 (Supplemental Table S1).

Among interacting protein partners of H3.3, we identified multiple subunits of the NuRD complex, including MTA1, MTA2, MTA3, HDAC1, HDAC2, CHD4, GATAD2B, MBD2, and RBBP4 by mass spectrometry (Supplemental Table S1; Fig. 1D). The interaction between H3.3 and NuRD subunits was severely compromised following mutation of lysine 4 to arginine, indicating a critical role of H3.3K4 in the interaction between NuRD and the H3.3 histone variant (Fig. 1D).

To further validate the interaction between H3.3 and NuRD as well as the involvement of H3.3K4, we immunoprecipitated wild-type and H3.3K4R mutant proteins followed by Western blotting with antibodies specific to NuRD subunits. Both wild-type H3.3 and H3.3K4R proteins were expressed at similar levels, and the induction of H3.3K4R expression did not change the expression of NuRD subunits, including MTA1, RBBP4, HDAC1, and HDAC2 (Fig. 2A, lanes 1–4). Although both wild-type H3.3 and H3.3K4R associated with similar levels of H2A.Z, H3.3K4R nucleosomes coprecipitated substantially less protein representing NuRD subunits compared to wild-type H3.3 (Fig. 2A, lanes 5–8).

To assess the role of H3.3K4 recognition in NuRD binding, pull-down binding assays with biotinylated H3 N-tail peptides with modified and unmodified lysine 4 were performed. To this end, whole-cell extract from MEF cells was incubated with

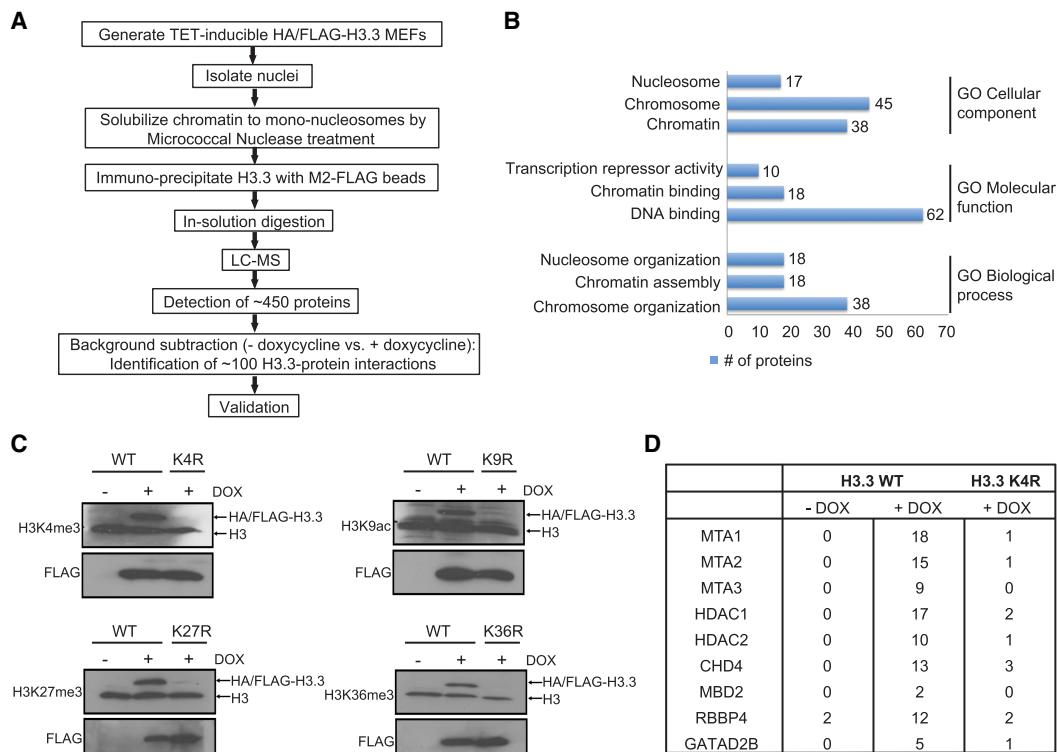


**Figure 1.** A H3.3-containing nucleosome immunoprecipitation followed by mass spectrometry identifies H3.3-interacting proteins. (A) Workflow for the identification of H3.3-nucleosome interacting proteins using an immunoprecipitation (IP)/mass spectrometry approach. (B) Gene Ontology analysis applied to the list of proteins coprecipitated with HA/FLAG-H3.3 and identified by mass spectrometry. (C) Western blots with lysate obtained from MEFs expressing wild-type and mutant versions of HA/FLAG-H3.3. Antibodies specific to histone H3 lysine modifications were used for immunoblotting and validation of lysine conversion to arginine. (D) Spectral counts associated with NuRD subunits obtained from HA/FLAG-H3.3 and HA/FLAG-H3.3K4R IPs.

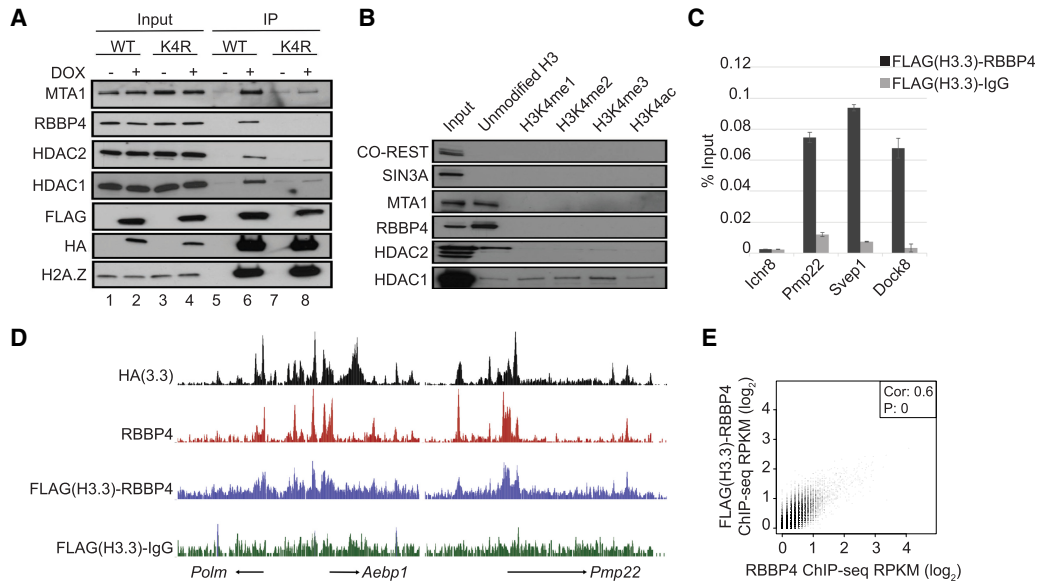


**Figure 2.** H3.3 interacts with the NuRD complex, and together, H3.3 and NuRD co-occupy many sites in the genome. (A) Validation of H3.3-NuRD interactions by co-immunoprecipitation. Lysate was obtained from MEF cells treated with (+) and without (–) doxycycline. HA/FLAG-H3.3 and HA/FLAG-H3.3K4R were immunoprecipitated with M2-FLAG resin prior to immunoblotting with antibodies specific to NuRD subunits. Five percent of total lysate was used as input. (B) Avidin-H3 N-tail peptide, either unmodified or modified at lysine 4, was incubated with MEF cell extract followed by SDS-PAGE with antibodies specific to various NuRD subunits. Five percent of total lysate was used as input. (C) Sequential FLAG-H3.3-RBBP4 and FLAG-H3.3-IgG ChIP-qPCR assays. Each qPCR reaction was performed in triplicate, and enrichment was normalized to input. Values are presented as means  $\pm$  SE. (D) Mapped reads from individual HA-H3.3 and RBBP4 ChIP-seq assays (top two lanes) as well as sequential FLAG-H3.3-RBBP4 and FLAG-H3.3-IgG ChIP-seq assays (bottom two lanes). (E) Correlation plots illustrating the relationship between FLAG-H3.3-RBBP4 and RBBP4 ChIP-seq levels across the genome.

immobilized H3 peptides. All NuRD subunits examined, with the exception of HDAC1, coprecipitated preferentially with the unmodified H3 tail (Fig. 2B). HDAC1 copurified weakly with unmodified H3 and its interaction with H3 became stronger with K4-methylated H3 indicating that other HDAC1-containing complexes may bind preferentially to modified H3 lysine 4. Together, these results suggest that lysine 4 is recognized by NuRD in its unmodified state and that both post-translational modification and conversion into arginine interfere with NuRD binding.

To test whether H3.3 and NuRD bind in a coordinate fashion to the same sites on chromatin, we performed sequential ChIP assays by using anti-FLAG antibody (H3.3) for the first ChIP and anti-RBBP4 antibody for the sequential ChIP. Indeed, both qPCR analysis for enrichment at select loci as well as NGS sequencing results confirmed that H3.3 and NuRD share many genomic loci (Fig. 2C,D). FLAG(H3.3)-RBBP4 levels correlated positively with RBBP4 ChIP-seq levels, demonstrating that our sequential ChIP-seq assay accurately captured RBBP4 levels, and also showing that RBBP4 levels alone can be considered representative of the level of the H3.3-RBBP4 interaction (Fig. 2E).

Multiple NuRD subunits also coprecipitated with immunopurified H3.1 (HA/FLAG-H3.1), suggesting that NuRD can recognize both H3.1 and H3.3 variants (Supplemental Table S2). We detected no peptides specific to H3.1 variants in HA/FLAG-H3.3 IPs and, vice versa, no peptides specific to H3.3 in HA/FLAG-H3.1 IPs, suggesting a homologous composition of nucleosomes in line with a previous report (Tagami et al. 2004). Although, the H3.3-specific chaperones ATRX and DAXX were found in complex with H3.3, we did not obtain spectral counts for HIRA peptides, suggesting that the HIRA chaperone may associate with H3.3 in a predeposition complex or, alternatively, that HIRA was expressed at levels too low to be detected by mass spectrometry.

### Genome-wide characterization of H3.3-NuRD interactions

Given the physical interaction between H3.3 and the NuRD complex, we set out to characterize their genome-wide distribution. For this purpose, we performed ChIP-seq assays for HA-H3.3 and NuRD subunits including CHD4, MBD2/3, MTA1, HDAC1, HDAC2, and RBBP4 (Fig. 3A). Analysis of H3.3 peak overlap with NuRD subunits revealed that around 63%–81% of NuRD-enriched regions (CHD4: 70%, MBD2/3: 63%, MTA1: 71%, HDAC1: 80%, HDAC2: 81%, RBBP4: 78% of peak overlap with H3.3) are co-occupied by H3.3 (Fig. 3B). We previously found that H3.3 is rapidly turned over at promoters and enhancers associated with active histone modifications H3K4me1, H3K27ac marks, and H2A.Z (Kraushaar et al. 2013). H3.3-NuRD peaks were numerous at gene promoters, intronic sites, and intergenic enhancers (Fig. 3C). In comparison to the total H3.3 distribution, peaks co-occupied by both H3.3 and NuRD were more prevalent at promoters and 5' UTR regions and less so within introns, 3' UTR regions, and downstream from promoters within gene body regions. As expected for a multiprotein complex such as NuRD, the relative enrichment distribution was similar across all NuRD subunits at various genomic sites (Fig. 3D). Although H3.3-NuRD peaks were numerous at intronic and intergenic sites, NuRD enrichment levels were only low to modest at these sites. In contrast, promoters co-occupied by H3.3 and NuRD carried high levels of NuRD enrichment.

Density plots across transcription start sites (TSSs) showed that NuRD subunits are strongly enriched  $\pm$ 1 kbp from the TSS, with highest enrichment over the nucleosome-depleted region. Density profiles generated from HA/FLAG-H3.3/RBBP4 sequential ChIP-seq samples revealed that co-occupancy is highest on either side of the nucleosome-depleted region (Fig. 3E).

The enrichment levels of NuRD subunits MTA1 and RBBP4 at promoter sites correlated positively with H3K4me3, H3K9ac, and

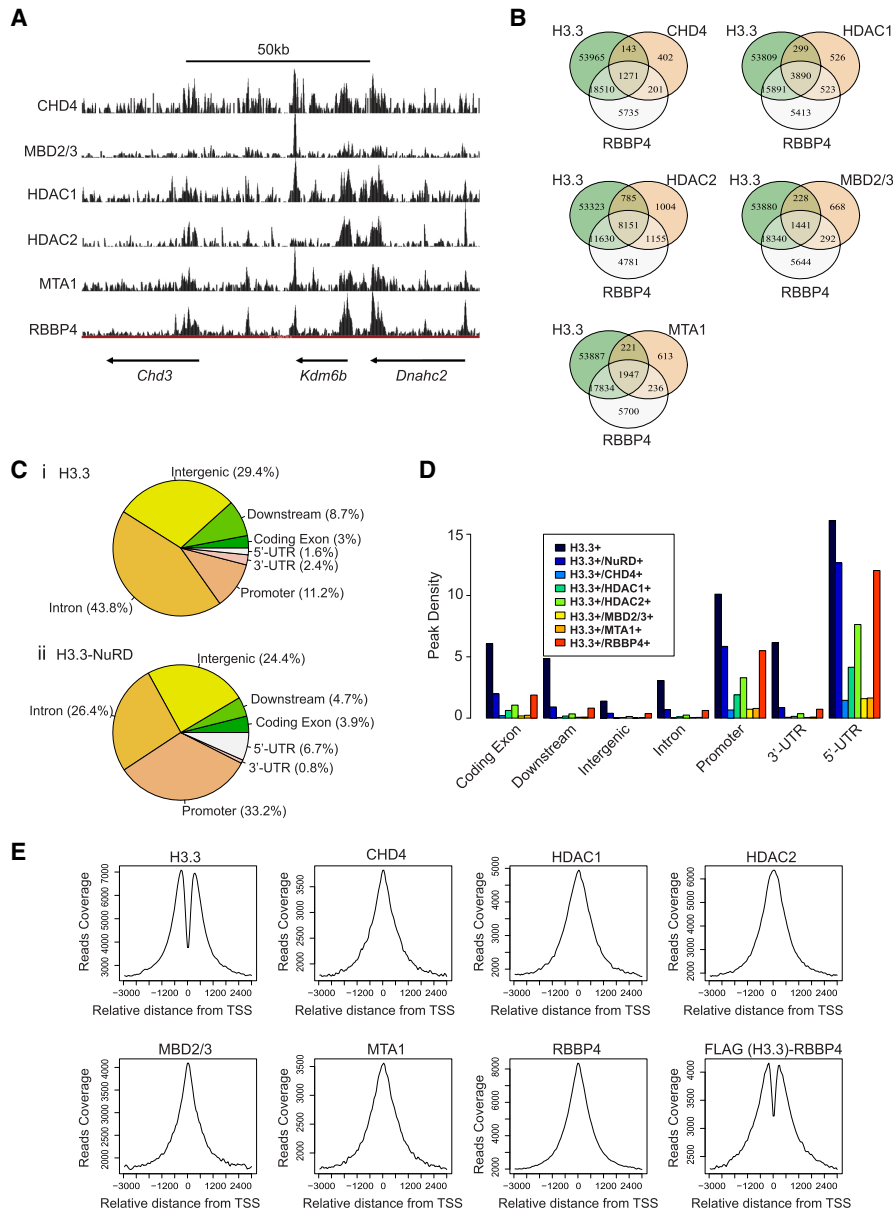


**Figure 3.** H3.3-NuRD interactions are prevalent at gene promoters. (A) Custom tracks generated from ChIP-seq data for NuRD subunits. (B) Venn diagrams illustrating overlap of enrichment between H3.3 and various NuRD subunits with  $P$ -value  $< 0.001$  for all subunits. (C) Pie chart illustrating the distribution of H3.3 peaks (i) and H3.3-NuRD peaks (ii) across various functional genomic regions. NuRD enrichment was defined as MTA1 and/or MBD2/3 peaks that overlap with RBBP4. (D) Bar graph illustrating the relative distribution of H3.3-NuRD interactions across various functional genomic regions. Enrichment levels were normalized over the total length of the genomic region. NuRD enrichment was defined as MTA1 and/or MBD2/3 peaks that overlap with RBBP4. (E) H3.3 and NuRD subunit enrichment profiles at  $\pm 3$  kbp of TSSs. Last panel depicts enrichment of H3.3/RBBP4 complexes generated from sequential FLAG-H3.3-RBBP4 ChIP-seq experiments.

H3K27ac marks as well as with the histone variants H2A.Z and H3.3, broadly indicating that NuRD recruitment is linked to gene activity (Fig. 4A). Direct examination of RNA-seq data confirmed this assumption and showed a positive correlation between gene activity and promoter occupancy for every NuRD subunit analyzed (Fig. 4B). To further investigate gene regulation by H3.3 and NuRD, we examined gene transcription at sites occupied by either H3.3 with or without NuRD. We observed higher transcription levels

for genes that are bound by both H3.3 and MTA1, or H3.3 and RBBP4 (Fig. 4C) compared to genes occupied by H3.3 only, suggesting that H3.3-NuRD co-occupation is a feature of actively transcribed genes and may indicate a modulatory role of NuRD rather than a role in gene silencing. Likewise, genes bound by NuRD only were, on average, transcribed at lower levels compared to genes occupied by NuRD and H3.3.

### Depletion of H3.3 leads to a decrease in NuRD recruitment

Next, we investigated the effect of loss of H3.3 on NuRD recruitment by comparing MTA1 and RBBP4 ChIP-seq profiles between wild-type and H3.3 knockdown cell lines. In mammalian cells, the histone variant H3.3 is encoded by two separate genes, *H3f3a* and *H3f3b*, whose transcription results in the same protein product. In order to ablate H3.3 protein expression, we used two separate short hairpin RNAs (shRNA) targeting both *H3f3a* and *H3f3b* transcripts, respectively (Fig. 5A). Despite efficient reduction in H3.3 protein, we observed modest but reproducible decreases in H2A.Z and histone marks that typically associate with H3.3, such as H3K36me3, H3K9ac, and H3K27ac. We observed no changes in H3K9me3 between wild-type and H3.3 knockdown lysates (Fig. 5B). Comparison of MTA1 and RBBP4 enrichment levels revealed a significant decrease in MTA1 globally (Fig. 5C, i) and at TSSs (Fig. 5C, ii). Likewise, RBBP4 binding decreased at all RBBP4 peaks (Fig. 5C, iii) as well as at TSSs (Fig. 5C, iv) following H3.3 knockdown, demonstrating that the association of NuRD with nucleosomes is to some extent dependent on histone variant deposition. ChIP-qPCR validation of ChIP-seq results confirmed reductions in MTA1 and RBBP4 levels at select sites following H3.3 knockdown (Supplemental Fig. S1).

In order to identify gene expression changes associated with loss of NuRD, we selected two wild-type and three H3.3 knockdown clonal cell populations with varying degrees of H3.3 knockdown efficiency and called differentially expressed genes based on changes in gene expression that correlate with the degree of H3.3 knockdown (Supplemental Fig. S2). Following H3.3 knockdown, we identified around 250 differentially expressed genes, of which 137 became down-regulated (Supplemental Fig. S2; Supplemental Table S3). Expression levels of MTA1 and RBBP4 themselves did not change substantially between wild-type and H3.3 knockdown cells, suggesting that reduced MTA1 and RBBP4

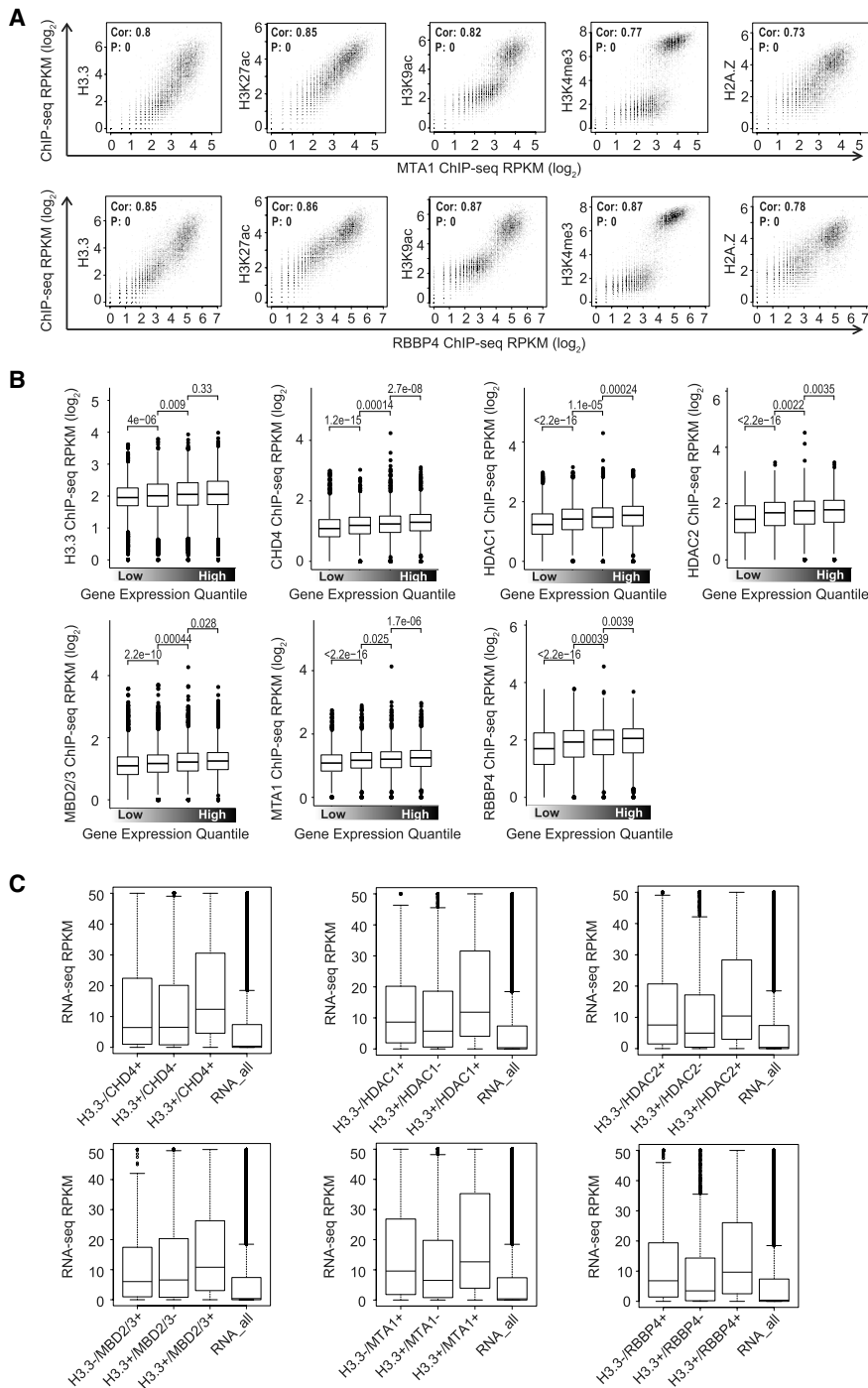


**Figure 4.** H3.3 and NuRD co-occupy promoters of actively transcribed genes. (A) Correlation plots illustrating the relationship between enrichment of RBBP4, MTA1, and levels of various histone marks enriched ±1 kbp of TSSs. (B) Genes were categorized based on their expression level from low to high using RNA-seq data. Median promoter enrichment of NuRD subunits was plotted for each category. (C) Box plots showing median expression levels for genes that are bound by H3.3, H3.3 and NuRD, and NuRD alone.

enrichment was due to lower levels of recruitment (Supplemental Fig. S2).

Genes that lost MTA1 and/or RBBP4 following H3.3 knock-down tended to exhibit lower expression on average, suggesting that the H3.3-NuRD interaction drives gene activation (Fig. 5D).

However, the average fold change differences in gene expression were relatively small, and hence we cannot rule out that H3.3 and NuRD individually carry out opposing roles as gene activator and repressor that may result in small net transcriptional changes.

## Discussion

NuRD, Co-REST, and Sin3A complexes represent the major H3 N-tail-binding proteins in nuclear extracts of mammalian cells (Nishioka et al. 2002; Zegerman et al. 2002; Wu et al. 2012; Kunowska et al. 2015). RBBP4 and RBBP7 have been identified as binding proteins of H3.3 previously (Goldberg et al. 2010). Here, we diagnostically identified an interaction between H3.3 and NuRD, including NuRD subunits that are shared between NuRD and other complexes like RBBP4 but also subunits unique to NuRD, such as MTA1, MTA2, MTA3, and MBD2.

Our finding that the K4R conversion on H3.3 abolishes NuRD binding in vivo indicates a key role for K4 in the interaction of H3.3 with histone binding proteins inside the NuRD complex (Musselman et al. 2009, 2012; Wu et al. 2013). Previous reports that have examined NuRD-H3 binding mechanisms are consistent with our results in that NuRD binds to unmodified H3 but not H3 methylated on lysine 4 (Zegerman et al. 2002; Wu et al. 2013). The inhibitory effect of K4 methylation on NuRD binding is surprising given our ChIP-seq results here and other studies that have shown strong enrichment of NuRD at sites enriched with H3K4me3 (Gunther et al. 2013; Menafra et al. 2014; Yang et al. 2016). It is conceivable that ChIP-seq results confounded by cell and nucleosome heterogeneity could falsely lead to the conclusion that NuRD may directly bind to H3K4-methylated nucleosomes in vivo. On the other hand, additional histone marks and/or chaperones specific to certain histone variants may override repulsive signals such as H3K4 methylation and still lead to recruitment of NuRD, albeit perhaps at lower affinity. It was recently shown that ZMYND8 (zinc finger MYND [Myeloid, Nerve, and DEAF-1]-type containing 8) selectively recruits NuRD to H3.1K36Me2/H4K16Ac and shows preference for H3.1 over H3.3, underscoring the importance of additional histone marks in NuRD recruitment (Adhikary et al. 2016; Spruijt et al. 2016). The exact determinants of NuRD binding will require further investigation, yet, this study shows that NuRD

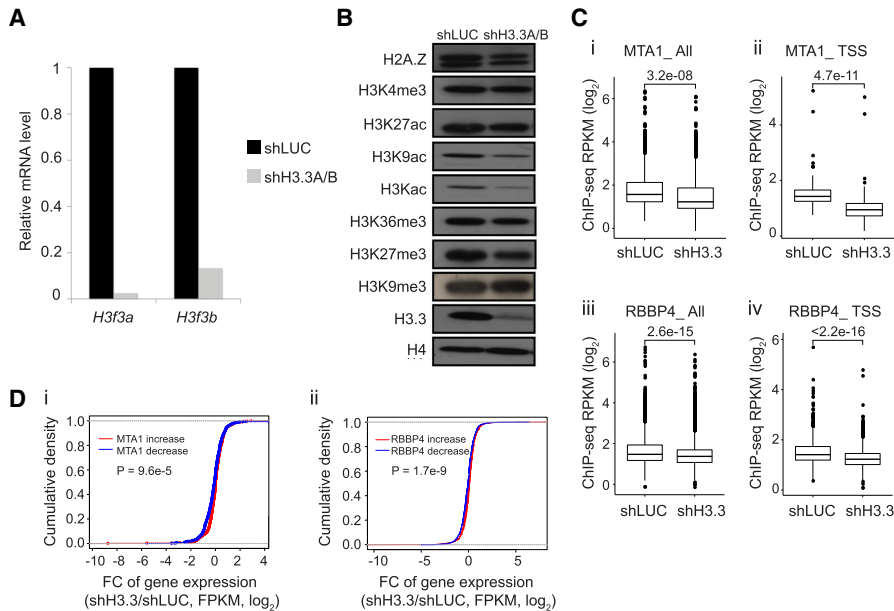


**Figure 5.** Knockdown of H3.3 leads to changes in global histone marks and a reduction in RBBP4 and MTA1 recruitment. (A) qRT-PCR assays allowing for comparison of *H3f3a* and *H3f3b* transcript levels between wild-type (LUC) and H3.3 knockdown cells. (B) Western blot showing changes in levels of histone modifications following knockdown of H3.3. The H3Kac antibody recognizes H3K9ac, H3K14ac, H3K18ac, H3K23ac, and H3K27ac. (C) Box plots showing changes in enrichment for MTA1 genome-wide (i) and  $\pm 1$  kbp of TSSs (ii), as well as changes in enrichment for RBBP4 genome-wide (iii) and  $\pm 1$  kbp of TSSs (iv) following knockdown of H3.3. (D) Empirical cumulative distribution for the fold change of gene expression (shH3.3/shLUC, FPKM,  $\log_2$ ), at sites that showed a decrease (blue line) or increase (red line) in MTA1 (i) and RBBP4 (ii) ChIP-seq levels. Genes with MTA1 (i) and RBBP4 (ii) enrichment  $\pm 1$  kbp from the TSS were included in this analysis. A decrease and increase in ChIP-seq levels after knockdown of H3.3 were defined as  $\log_2FC < -0.5$  and  $\log_2FC > 0.5$ , respectively.

recruitment cannot be fully compensated for when H3.3 is lost altogether.

ChIP-seq experiments with antibodies specific to various NuRD subunits revealed that the majority of NuRD-enriched sites are co-enriched in H3.3. Considering the ubiquitous expression of both H3.3 and NuRD, their functions as gene activators and repressors, respectively, as well as their roles in cancer pathology renders the H3.3-NuRD interaction of particular importance to the modulation of gene transcription. NuRD activity is generally thought of as a factor mediating gene repression through histone deacetylation. Nevertheless genome-wide mapping of NuRD subunits by us and others have revealed NuRD binding at active promoters. Menafra et al. (2014) reported binding of tagged MBD2 in MCF-7 breast cancer cells at hypermethylated sites but also a subset of active genes transcribed at low levels. It has been claimed that NuRD/MBD2 binds primarily at repressed and hypermethylated genes and NuRD/MBD3 predominantly at active genes devoid of methylation (Gunther et al. 2013). However recent studies have revealed a highly overlapping localization of MBD2 and MBD3 binding sites independent of methylation status in favor of a synergistic role of MBD2 and MBD3 (Hainer et al. 2016). Our genome-wide profiling of multiple NuRD subunits showed that NuRD localizes at moderately to highly transcribed genes that are co-occupied by H3.3, indicating cell-type-specific differences in NuRD distribution.

Functional studies that have utilized depletion of MBD2 and MBD3 failed to unambiguously support a unifying role for NuRD as a gene repressor. MBD2 knockdown in erythrocytes resulted in re-expression of the  $\rho$ -globin gene which is methylated and

bound by MBD2 and MTA1 (Kransdorf et al. 2006). Depletion of MBD2 by RNAi in HeLa cells resulted in a roughly equal number of up- and down-regulated genes (Gunther et al. 2013). Interdependent binding of NuRD and epigenetic regulators involved in gene activation may explain why functional studies have not provided clear answers. In ES cells, a subset of actively transcribed genes are bound by both BRG1 and MBD3, which each antagonistically activate and repress gene expression of their targets, respectively (Yildirim et al. 2011). Hence, H3.3 deposition may be a precursor for recruitment of both NuRD and gene activators that act to keep transcription levels in check.

Despite efficient knockdown of H3.3 through knockdown of both *H3f3a* and *H3f3b*, we only observed moderate changes in the levels of histone marks as well as in the number of differentially expressed genes, considering the widespread distribution of H3.3. Studies that have used *H3f3b* KO MEFs as well as HIRA knockout ES cells have also reported moderate changes in histone modifications and small changes in global gene expression (Goldberg et al. 2010; Bush et al. 2013). It seems likely that post-translational modifications can be partially maintained and compensated

for by canonical H3. Regardless, we cannot fully rule out the possibility that the remaining base level of H3.3 protein left following knockdown is sufficient to carry out transcription-related functions.

In summary, we identified a prominent interaction between H3.3 and NuRD, which takes place at promoters of actively transcribed genes and regulatory sites occupied by H3.3. We deciphered that the physical interaction between H3.3 and NuRD subunits is critically dependent upon unmodified Lys4 of the H3.3 N-tail. Furthermore, loss of H3.3 led to a global reduction in NuRD binding, suggesting that the deposition of H3.3 and NuRD recruitment are directly linked processes. Deposition of H3.3 in place of canonical histones may direct NuRD to promoters of actively transcribed genes and prevent disproportionate Pol II-dependent transcription.

## Methods

### Cell culture, cell line derivation, and RNAi

NIH/3T3 Tet-On 3G MEFs (Clontech) were cultured in standard conditions with medium containing 10% FBS. A modified *H3f3b* coding sequence was subcloned in-frame with an HA and FLAG tag at the C terminus and cloned into the lentiviral pLVX-Tight-Puro Vector (Clontech). Lysine residues were converted to arginines at amino acid positions K4, K9, K27, and K36, and mutations were validated by Sanger sequencing.

The RNA interference constructs targeting H3.3 were generated by inserting *H3f3a* and *H3f3b* target sequences into pGreenPuro

Lentivector (System Biosciences) constructs. The sequences used to knock down *H3f3a* and *H3f3b* were 5'-GATACCAATCTGTGTGCTATCCATGCCAA-3' and 5'-GATACCAATCTGTGTGCCATCCACGCCAA-3', respectively.

The control construct was made by inserting a luciferase sequence 5'-GTGCGTGTAGTACTAATCCTATTT-3' into the pGreenPuro Lentivector. Lentiviral particles were packaged in 293T cells with the psPAX2 packaging plasmid. Subsequently, we transduced NIH/3T3 Tet-On 3G MEFs (Clontech) and drug-selected with puromycin for stable integration.

### Mononucleosomal immunoprecipitation

HA/FLAG-H3.3-expressing NIH/3T3 fibroblasts (Kraushaar et al. 2013) were cultured with and without 2  $\mu$ g/mL doxycycline.  $1.5 \times 10^8$  cells were collected and processed according to Draker et al. (2012). Briefly, cell pellets were suspended in 5 mL of Buffer A (20 mM HEPES at pH 7.5, 10 mM KCl, 1.5 mM MgCl<sub>2</sub>, 0.34 M sucrose, 10% glycerol, 1 mM dithiothreitol, 5 mM sodium butyrate, 10 mM NEM, protease inhibitors), pelleted, resuspended in 5 mL of Buffer A containing 0.2% Triton X-100, and incubated for 5 min on ice. Nuclei were washed in 5 mL of Cutting Buffer (10 mM Tris-HCl at pH 7.5, 15 mM NaCl, sodium butyrate, and protease inhibitors), pelleted, and subsequently resuspended in Cutting Buffer plus 2 mM CaCl. Micrococcal nuclease (Roche) was added at a concentration of 10 units per  $10^7$  cells and the reaction incubated for 30 min at 37°C, at which point the reaction was stopped through addition of EGTA (10 mM final concentration). The cell suspension was transferred to TE pH 8.0, briefly sonicated, and incubated for 15 min on ice to induce hypotonic lysis. The salt concentration of the nuclear suspension was adjusted by adding 3 $\times$  Buffer D (60 mM HEPES at pH 7.5, 450 mM NaCl, 4.5 mM MgCl<sub>2</sub>, 0.6 mM EGTA, 0.6% Triton X-100, 30% glycerol) dropwise with continuous vortexing. Following centrifugation at 16,000g for 10 min, the supernatant was transferred to a new tube and 300  $\mu$ L of M2-FLAG resin was added and incubated at 4°C overnight.

### Mass spectrometry

Eluted proteins from the M2-agarose beads in 8 M urea buffer were subjected to an in-solution digestion procedure. Briefly, the proteins were reduced using dithiothreitol (DTT, Sigma 43815) for 1 h at 37°C and then alkylated using iodoacetamide at room temperature (IAA, Sigma I1149). Samples were diluted using ammonium bicarbonate to reduce the urea concentration to <0.8 M and later digested overnight at 37°C with 2  $\mu$ g of trypsin enzyme, sequencing grade (Promega, V5111). The resulting tryptic peptides were acidified using formic acid to pH <3 and the samples were desalted and concentrated using C18 zip-tips (Millipore Corporation, ZTC18S096).

Liquid chromatography tandem mass spectrometry was performed using an Eksigent nano-LC-Ultra 1D Plus system coupled to an LTQ-Orbitrap Elite mass spectrometer (Thermo Fisher Scientific) using CID (collision-induced dissociation) fragmentation. Peptides were first loaded onto a Zorbax 300SB-C18 trap column (Agilent) at a flow rate of 6  $\mu$ L/min for 6 min and then separated on a reversed-phase Picofrit analytical column (New Objective) using a 65-min linear gradient of 5%–35% acetonitrile in 0.1% formic acid at a flow rate of 250 nL/min. LTQ-Orbitrap Elite settings were as follows: spray voltage, 1.5 kV; full MS range, m/z 300–2000. The LTQ-Orbitrap Elite was operated in a data-dependent mode, i.e., one MS1 high resolution scan for precursor ions followed by six data-dependent MS2 scans for precursor ions above a threshold ion count of 500 with collision energy of 35%.

### Protein identification

The raw files generated from the LTQ Orbitrap Elite were analyzed using Proteome Discoverer version 1.4 software (Thermo Fisher Scientific). Data were submitted to the Mascot v2.5.1 (Matrix Sciences) search engine with the following search criteria; database, Swiss-Prot (Swiss Institute of Bioinformatics); taxonomy, mouse; enzyme, trypsin; miscleavages, 2; variable modifications, oxidation (M), deamidation (NQ), methylation (K); fixed modification, carbamidomethyl (C); MS peptide tolerance 20 ppm; MS/MS tolerance 0.8 Da. The resulting data file was loaded into the Scaffold software (version scaffold\_4.3.4, Proteome Software, Inc.) to filter and quantitate the peptides and proteins. For protein identification, filters were set to at least one unique peptide identified per protein with an FDR setting of 0.5%. Data analysis and clustering were performed in the Scaffold software. Relative quantification was done in a label-free approach with the setting Quantitative Value (Normalized Total Spectra). For comparison, the total number of spectral counts identified for each protein was visualized and compared to the counterpart. Spectral counts of the control (minus doxycycline) samples were considered background and were used to remove false positive protein identifications. For semiquantitative comparison across samples, spectral counts were normalized to total nucleosome content based off histone H4 spectral counts. Duplicate analyses for HA/FLAG-H3.3 wild-type and HA/FLAG-H3.3 mutants were compared and only proteins with differences in spectral counts greater than twofold in both data sets were considered as differential interactions, given a minimum spectral count of 2 in wild-type samples.

For validation by co-immunoprecipitation, protein was eluted with SDS sample buffer and run on a 10% SDS-gel. Antibodies used for immunoblotting: HDAC2 (Abcam, ab7029), HDAC1 (Abcam, ab7028), RBBP4 (Abcam, ab79416), MTA1 (Santa Cruz, sc-9446), HA (Roche, 11666606001), FLAG (M2, Sigma, F1804), MBD2/3 (Abcam, ab45027), H3.3 (Millipore, 09–838), H3K4me3 (Millipore, 17–614), H3K9ac (Abcam, ab4441), H3K27ac (Abcam, ab4729), H3Kac (Abcam, ab47915), H3K27me3 (Millipore, 07–449), H3K36me3 (Abcam, ab9050), H2A.Z (Abcam, ab4147), H3K9me3 (Abcam, ab8898), H4 (Abcam, ab7311). Histones were isolated by acid extraction as described in Shechter et al. (2007) prior to immunoblotting against H3.3 and histone modifications.

### Histone peptide pull-down assay

One hundred micrograms of lyophilized histone peptides (H3K4ac, Epicpyher; unmodified H3, H3K4me1, H3K4me2, H3K4me3; Millipore) were dissolved in 400  $\mu$ L of PBS.  $1 \times 10^8$  MEFs were hypotonically lysed with Buffer A (10 mM HEPES at pH 7.9, 1.5 mM MgCl<sub>2</sub>, 10 mM KCl, freshly added protease inhibitors and DTT to 1 mM) before nuclear extract was isolated with Buffer C (20 mM HEPES at pH 7.9, 25% v/v glycerol, 420 mM KCl, 1.5 mM MgCl<sub>2</sub>, 0.2 mM EDTA, freshly added protease inhibitors and DTT to 1 mM) and the salt concentration lowered to 150 mM using Buffer D (20 mM HEPES at pH 7.9, 20% v/v glycerol, 0.2 mM EDTA, 0.2% Triton X-100). Following mechanical lysis by sonication, 50  $\mu$ L of prewashed avidin-histone peptide slurry was added to precleared lysate and incubated overnight at 4°C. After washing of the avidin beads, SDS sample buffer was added and samples were boiled for 5 min and subsequently run on a 10% SDS gel. The following antibodies were used for the histone peptide pull-down assay: mSin3A (Abcam, ab3479), CoREST (Millipore, 07–455), HDAC2 (Abcam, ab7029), HDAC1 (Abcam, ab7028), RBBP4 (Abcam, ab79416), MTA1 (Santa Cruz, sc-9446).

## ChIP and deep sequencing library preparation

ChIP-seq experiments were performed as described previously (Barski et al. 2007) with the following antibodies: MBD2/3 (Abcam, ab45027), CHD4 (Abcam, ab70469), HDAC2 (Abcam, 7029), HDAC1 (Abcam, ab7028), RBBP4 (Abcam, ab79416).

For sequential ChIP,  $4 \times 10^7$  cells were lysed, and crosslinked DNA was subjected to immunoprecipitation with 50  $\mu$ L of M2-FLAG agarose (Sigma). Agarose beads were washed twice with RIPA buffer, resuspended in 100  $\mu$ L TE, followed by elution of the immunocomplexes with 3  $\mu$ L of 5  $\mu$ g/ $\mu$ L FLAG peptide (Sigma-Aldrich, F3290) at 4°C for 2 h. The supernatant was transferred and re-immunoprecipitated with RBBP4 antibody (Abcam, ab79416) immobilized to Dynabeads Protein A (Thermo Fisher Scientific) before crosslinking was reversed and protein digested with Proteinase G.

ChIP material was blunt-ended and phosphorylated with the End-it-Repair kit (EPICENTRE). Illumina genome sequencing adaptors were ligated with T4 DNA ligase (New England Biolabs) after addition of adenosine nucleotides, using exo-Klenow. Samples were PCR-amplified with multiplexed Illumina genomic DNA sequencing primers. PCR products (250 to 450 bp in size) were gel-purified and submitted for Illumina deep sequencing.

For RNA-seq library construction, polyadenylated RNA was isolated from 5  $\mu$ g of total RNA isolated using the Dynabeads mRNA Direct kit (Invitrogen). Double-stranded cDNA was generated with the Double-stranded cDNA synthesis kit (Invitrogen), sonicated, and subsequently processed exactly like ChIP DNA.

## qRT-PCR

Total RNA was isolated using the RNeasy kit (Qiagen), and cDNA was made from 1  $\mu$ g of total RNA using the SuperScript III First-Strand Synthesis System (Invitrogen). RT-PCR was performed with the following primers: *H3f3a* (F): TTTTCCATGGGGTCA AAGG; *H3f3a* (R): TCACACACAAATGAACGTGG; *H3f3b* (F): CAC TCAGGATGAATGGGAAGA; *H3f3b* (R): CCCATCCCTTCTGCGT ATTA.

ChIP-qPCR signals were calculated as percent input with error bars representing standard errors ( $n=3$ ). ChIP-PCR was performed with the following primers: *Ichr8* Forward: AAGGGCCTCTGC TTA AAAA, *Ichr8* Reverse: AGAGCTCCATGGCAGGTAGA; *Pmp22* Forward: CAGACTCAATCAGCCTCTTACG, *Pmp22* Reverse: CT ATCCCTTGGTTGCTGCTG; *Cnm3* Forward: CCGGCACTGTCC TAGACTTC, *Cnm3* Reverse: AGAGCATGTCCACGATGTTG; *Fzd2* Forward: ATCTCCATCCCGGACCAC, *Fzd2* Reverse: CTGGT GTAGGCGATGTCC; *Svep1* Forward: ACGACTCGTCCACCAG GA, *Svep1* Reverse: AGCAGGGAGCAAAGTGGA; *Atoh8* Forward: TGTGTCTGTCCCGAAGC, *Atoh8* Reverse: AACTTTCCGATTGG ACTTGG; *Dock8* Forward: CGCTCAAGATCAACAGGTAAGA, *Dock8* Reverse: CAAGAGGACGAGAATGAGTCCG.

## Genome mapping, peak calling, and annotation

ChIP-seq reads of each library were mapped to the mouse genome (UCSC mm9) (Kent et al. 2002) from the Illumina iGenome database ([http://support.illumina.com/sequencing/sequencing\\_software/igenome.html](http://support.illumina.com/sequencing/sequencing_software/igenome.html)) using Bowtie (Langmead et al. 2009). Redundant mapped reads were removed. The Model-based Analysis of ChIP-Seq (MACS) (Zhang et al. 2008) version 1.4.2 was used to call peaks with default parameters of model fold between 10 and 30 and a *P*-value cutoff of  $1.00 \times 10^{-5}$ . Overlapping peaks of NuRD subunits and H3.3 were merged using the Merge function of the BEDTools package (Quinlan 2014) in order to generate a reference peak set. Then, each reference peak was annotated to a certain genomic category if its center overlapped with a certain

RefSeq genomic region, i.e., exon, intron, promoter (3 kbp upstream of TSS), 3' UTR, 5' UTR, and downstream regions (5 kbp downstream from transcription end site, TES). The RefSeq genomic annotation of mm9 was downloaded from the UCSC Genome Browser.

## ChIP-seq enrichment calculation

A 1 kbp window table for all chromosomes of the mouse genome was generated using the Makewindows function of the BEDTools package. A  $\pm 1$  kbp window table for each TSS was generated using the Makewindows and Slop functions of the BEDTools package along with a TSS location table downloaded from the UCSC Genome Browser. The tag count for each window was then calculated using the IntersectBed function of the BEDTools package. Finally, the RPKM value for each window was generated with the tag count normalized against the number of total mapped reads of the corresponding ChIP-seq library.

## TSS profile generation

Using the foregoing methods,  $\pm 3$  kbp windows on all TSS regions were generated. Then, each TSS window was divided into 50-bp bins. The coverage level of each bin was calculated by adding up the number of mapped reads for all gene isoforms at the same relative location for each ChIP-seq library using the IntersectBed function of the BEDTools package.

## Gene expression analysis

The reads from RNA-seq libraries were mapped to the mouse genome (mm9) using TopHat (Trapnell et al. 2009). The gene expression level for each gene and gene isoform was then measured with the expected number of fragments per kilobase of transcript sequence per millions base pairs sequenced (FPKM) using Cufflinks (Trapnell et al. 2012). Differentially expressed genes were identified with the following criteria:  $\text{FPKM}(\text{shLUC} \#1) \leq \text{FPKM}(\text{shH3.3A/B} \#1) \leq \text{FPKM}(\text{shH3.3A/B} \#2) \leq \text{FPKM}(\text{shH3.3A/B} \#3)$  and  $\text{FPKM}(\text{shLUC} \#2) \leq \text{FPKM}(\text{shH3.3A/B} \#1) \leq \text{FPKM}(\text{shH3.3A/B} \#2) \leq \text{FPKM}(\text{shH3.3A/B} \#3)$  or  $\text{FPKM}(\text{shLUC} \#1) \geq \text{FPKM}(\text{shH3.3A/B} \#1) \geq \text{FPKM}(\text{shH3.3A/B} \#2) \geq \text{FPKM}(\text{shH3.3A/B} \#3)$  and  $\text{FPKM}(\text{shLUC} \#2) \geq \text{FPKM}(\text{shH3.3A/B} \#1) \geq \text{FPKM}(\text{shH3.3A/B} \#2) \geq \text{FPKM}(\text{shH3.3A/B} \#3)$ .

## Conjoint analysis of gene expression and RBBP4/MTA1 ChIP-seq levels in wild-type and H3.3 knockdown samples

The FPKM value for each gene isoform was evaluated using Cufflinks for shLUC #1/2 and shH3.3A/B #3 RNA-seq libraries. RBBP4 and MTA1 ChIP-seq levels were calculated as RPKM values at each  $\pm 1$  kbp TSS region as above using the BEDTools package. The cumulative density curves were each generated for gene isoforms that displayed an increase or decrease in ChIP-seq levels at their TSS regions.

## Data access

ChIP-seq and RNA-seq level data from this study have been submitted to the NCBI Gene Expression Omnibus (GEO; <http://www.ncbi.nlm.nih.gov/geo>) under accession number GSE110382. Sequence data from this study have been submitted to the NCBI Sequence Read Archive (SRA; <https://www.ncbi.nlm.nih.gov/sra>) under accession number SRP133189. Sanger sequencing data for cDNAs have been submitted to the NCBI GenBank (<https://www.ncbi.nlm.nih.gov/genbank/>) under accession numbers MH899003, MH899004, MH899005, MH899006, and

MH899007. Mass spectrometry data from this study have been submitted to the Peptide Atlas (<http://peptideatlas.org>) under accession number PASS01232.

## Acknowledgments

We thank the National Heart, Lung, and Blood Institute (NHLBI) DNA Sequencing Core facility for sequencing the ChIP-seq and RNA-seq libraries. We thank the NHLBI Proteomics Core facility, in particular, Marjan Gucek and Sajni Patel, for their assistance in the mass spectrometry analysis. We thank Drs. Binbin Lai and Gangqing Hu for their help with the manuscript preparation and data deposition. The work was supported by the Division of Intramural Research, NHLBI, National Institutes of Health, USA (grant number HL005801-08).

*Author contributions:* D.C.K. participated in the design of the study, carried out experiments, and wrote the manuscript. Z.C. carried out the data analysis. K.C. generated libraries for NuRD subunits. Q.T. contributed to the generation of constructs. J.Z. participated in the data analysis and directed the study. K.Z. conceived the study, participated in its design and coordination, wrote the manuscript, and directed the study. All authors read and approved the final manuscript.

## References

- Adhikary S, Sanyal S, Basu M, Sengupta I, Sen S, Srivastava DK, Roy S, Das C. 2016. Selective recognition of H3.1K36 dimethylation/H4K16 acetylation facilitates the regulation of all-*trans*-retinoic acid (ATRA)-responsive genes by putative chromatin reader ZMYND8. *J Biol Chem* **291**: 2664–2681.
- Ahmad K, Henikoff S. 2002. The histone variant H3.3 marks active chromatin by replication-independent nucleosome assembly. *Mol Cell* **9**: 1191–1200.
- Barski A, Cuddapah S, Cui K, Roh TY, Schones DE, Wang Z, Wei G, Chepelev I, Zhao K. 2007. High-resolution profiling of histone methylations in the human genome. *Cell* **129**: 823–837.
- Basta J, Rauchman M. 2015. The nucleosome remodeling and deacetylase complex in development and disease. *Transl Res* **165**: 36–47.
- Bush KM, Yuen BT, Barrilleaux BL, Riggs JW, O'Geen H, Cotterman RF, Knoepfler PS. 2013. Endogenous mammalian histone H3.3 exhibits chromatin-related functions during development. *Epigenetics Chromatin* **6**: 7.
- Draker R, Ng MK, Sarcinella E, Ignatchenko V, Kislinger T, Cheung P. 2012. A combination of H2A.Z and H4 acetylation recruits Brd2 to chromatin during transcriptional activation. *PLoS Genet* **8**: e1003047.
- Elsaesser SJ, Goldberg AD, Allis CD. 2010. New functions for an old variant: no substitute for histone H3.3. *Curr Opin Genet Dev* **20**: 110–117.
- Fujita N, Jaye DL, Geigerman C, Akyildiz A, Mooney MR, Boss JM, Wade PA. 2004. MTA3 and the Mi-2/NuRD complex regulate cell fate during B lymphocyte differentiation. *Cell* **119**: 75–86.
- Goldberg AD, Banaszynski LA, Noh KM, Lewis PW, Elsaesser SJ, Stadler S, Dewell S, Law M, Guo X, Li X, et al. 2010. Distinct factors control histone variant H3.3 localization at specific genomic regions. *Cell* **140**: 678–691.
- Gong F, Clouaire T, Aguirrebengoa M, Legube G, Miller KM. 2017. Histone demethylase KDM5A regulates the ZMYND8–NuRD chromatin remodeler to promote DNA repair. *J Cell Biol* **216**: 1959–1974.
- Gunther K, Rust M, Leers J, Boettger T, Scharfe M, Jarek M, Bartkuhn M, Renkawitz R. 2013. Differential roles for MBD2 and MBD3 at methylated CpG islands, active promoters and binding to exon sequences. *Nucleic Acids Res* **41**: 3010–3021.
- Ha M, Kraushaar DC, Zhao K. 2014. Genome-wide analysis of H3.3 dissociation reveals high nucleosome turnover at distal regulatory regions of embryonic stem cells. *Epigenetics Chromatin* **7**: 38.
- Hainer SJ, McCannell KN, Yu J, Ee LS, Zhu LJ, Rando OJ, Fazzio TG. 2016. DNA methylation directs genomic localization of Mbd2 and Mbd3 in embryonic stem cells. *eLife* **5**: e21964.
- Hake SB, Garcia BA, Duncan EM, Kauer M, Dellaire G, Shabanowitz J, Bazett-Jones DP, Allis CD, Hunt DF. 2006. Expression patterns and post-translational modifications associated with mammalian histone H3 variants. *J Biol Chem* **281**: 559–568.
- Henikoff S, McKittrick E, Ahmad K. 2004. Epigenetics, histone H3 variants, and the inheritance of chromatin states. *Cold Spring Harb Symp Quant Biol* **69**: 235–243.
- Hu G, Cui K, Northrup D, Liu C, Wang C, Tang Q, Ge K, Levens D, Crane-Robinson C, Zhao K. 2013. H2A.Z facilitates access of active and repressive complexes to chromatin in embryonic stem cell self-renewal and differentiation. *Cell Stem Cell* **12**: 180–192.
- Jin C, Felsenfeld G. 2007. Nucleosome stability mediated by histone variants H3.3 and H2A.Z. *Genes Dev* **21**: 1519–1529.
- Jin C, Zang C, Wei G, Cui K, Peng W, Zhao K, Felsenfeld G. 2009. H3.3/H2A.Z double variant-containing nucleosomes mark 'nucleosome-free regions' of active promoters and other regulatory regions. *Nat Genet* **41**: 941–945.
- Kaji K, Caballero IM, MacLeod R, Nichols J, Wilson VA, Hendrich B. 2006. The NuRD component Mbd3 is required for pluripotency of embryonic stem cells. *Nat Cell Biol* **8**: 285–292.
- Kent WJ, Sugnet CW, Furey TS, Roskin KM, Pringle TH, Zahler AM, Haussler D. 2002. The human genome browser at UCSC. *Genome Res* **12**: 996–1006.
- Kim TW, Kang BH, Jang H, Kwak S, Shin J, Kim H, Lee SE, Lee SM, Lee JH, Kim JH, et al. 2015. Ctbp2 modulates NuRD-mediated deacetylation of H3K27 and facilitates PRC2-mediated H3K27me3 in active embryonic stem cell genes during exit from pluripotency. *Stem Cells* **33**: 2442–2455.
- Kransdorf EP, Wang SZ, Zhu SZ, Langston TB, Rupon JW, Ginder GD. 2006. MBD2 is a critical component of a methyl cytosine-binding protein complex isolated from primary erythroid cells. *Blood* **108**: 2836–2845.
- Kraushaar DC, Zhao K. 2013. The epigenomics of embryonic stem cell differentiation. *Int J Biol Sci* **9**: 1134–1144.
- Kraushaar DC, Jin W, Maunakea A, Abraham B, Ha M, Zhao K. 2013. Genome-wide incorporation dynamics reveal distinct categories of turnover for the histone variant H3.3. *Genome Biol* **14**: R121.
- Kunowska N, Rotival M, Yu L, Choudhary J, Dillon N. 2015. Identification of protein complexes that bind to histone H3 combinatorial modifications using super-SILAC and weighted correlation network analysis. *Nucleic Acids Res* **43**: 1418–1432.
- Langmead B, Trapnell C, Pop M, Salzberg SL. 2009. Ultrafast and memory-efficient alignment of short DNA sequences to the human genome. *Genome Biol* **10**: R25.
- Lewis PW, Elsaesser SJ, Noh KM, Stadler SC, Allis CD. 2010. Daxx is an H3.3-specific histone chaperone and cooperates with ATRX in replication-independent chromatin assembly at telomeres. *Proc Natl Acad Sci* **107**: 14075–14080.
- Li DQ, Kumar R. 2015. Unravelling the complexity and functions of MTA coregulators in human cancer. *Adv Cancer Res* **127**: 1–47.
- Maze I, Wenderski W, Noh KM, Bagot RC, Tzavaras N, Purushothaman I, Elsaesser SJ, Guo Y, Ionete C, Hurd YL, et al. 2015. Critical role of histone turnover in neuronal transcription and plasticity. *Neuron* **87**: 77–94.
- Menafrá R, Brinkman AB, Matarese F, Franci G, Bartels SJ, Nguyen L, Shimbo T, Wade PA, Hubner NC, Stunnenberg HG. 2014. Genome-wide binding of MBD2 reveals strong preference for highly methylated loci. *PLoS One* **9**: e99603.
- Musselman CA, Mansfield RE, Garske AL, Davrazou F, Kwan AH, Oliver SS, O'Leary H, Denu JM, Mackay JP, Kutateladze TG. 2009. Binding of the CHD4 PHD2 finger to histone H3 is modulated by covalent modifications. *Biochem J* **423**: 179–187.
- Musselman CA, Ramirez J, Sims JK, Mansfield RE, Oliver SS, Denu JM, Mackay JP, Wade PA, Hagman J, Kutateladze TG. 2012. Bivalent recognition of nucleosomes by the tandem PHD fingers of the CHD4 ATPase is required for CHD4-mediated repression. *Proc Natl Acad Sci* **109**: 787–792.
- Nishioka K, Chuikov S, Sarma K, Erdjument-Bromage H, Allis CD, Tempst P, Reinberg D. 2002. Set9, a novel histone H3 methyltransferase that facilitates transcription by precluding histone tail modifications required for heterochromatin formation. *Genes Dev* **16**: 479–489.
- Quinlan AR. 2014. BEDTools: the Swiss-army tool for genome feature analysis. *Curr Protoc Bioinformatics* **47**: 11.12.1–34.
- Rais Y, Zviran A, Geula S, Gafni O, Chomsky E, Viukov S, Mansour AA, Caspi I, Krupalnik V, Zerbib M, et al. 2013. Deterministic direct reprogramming of somatic cells to pluripotency. *Nature* **502**: 65–70.
- Ray-Gallet D, Quivy JP, Scamps C, Martini EM, Lipinski M, Almouzni G. 2002. HIRA is critical for a nucleosome assembly pathway independent of DNA synthesis. *Mol Cell* **9**: 1091–1100.
- Ray-Gallet D, Woolfe A, Vassias I, Pellentz C, Lacoste N, Puri A, Schultz DC, Pchelintsev NA, Adams PD, Jansen LE, et al. 2011. Dynamics of histone H3 deposition in vivo reveal a nucleosome gap-filling mechanism for H3.3 to maintain chromatin integrity. *Mol Cell* **44**: 928–941.
- Shechter D, Dormann HL, Allis CD, Hake SB. 2007. Extraction, purification and analysis of histones. *Nat Protoc* **2**: 1445–1457.
- Spruijt CG, Luijsterburg MS, Menafrá R, Lindeboom RG, Jansen PW, Edepuganti RR, Baltissen MP, Wiegant WW, Voelker-Albert MC,

- Matarese F, et al. 2016. ZMYND8 co-localizes with NuRD on target genes and regulates poly(ADP-ribose)-dependent recruitment of GATAD2A/ NuRD to sites of DNA damage. *Cell Rep* **17**: 783–798.
- Szenker E, Lacoste N, Almouzni G. 2012. A developmental requirement for HIRA-dependent H3.3 deposition revealed at gastrulation in *Xenopus*. *Cell Rep* **1**: 730–740.
- Tagami H, Ray-Gallet D, Almouzni G, Nakatani Y. 2004. Histone H3.1 and H3.3 complexes mediate nucleosome assembly pathways dependent or independent of DNA synthesis. *Cell* **116**: 51–61.
- Tamura T, Smith M, Kanno T, Dasenbrock H, Nishiyama A, Ozato K. 2009. Inducible deposition of the histone variant H3.3 in interferon-stimulated genes. *J Biol Chem* **284**: 12217–12225.
- Torchy MP, Hamiche A, Klaholz BP. 2015. Structure and function insights into the NuRD chromatin remodeling complex. *Cell Mol Life Sci* **72**: 2491–2507.
- Trapnell C, Pachter L, Salzberg SL. 2009. TopHat: discovering splice junctions with RNA-Seq. *Bioinformatics* **25**: 1105–1111.
- Trapnell C, Roberts A, Goff L, Pertea G, Kim D, Kelley DR, Pimentel H, Salzberg SL, Rinn JL, Pachter L. 2012. Differential gene and transcript expression analysis of RNA-seq experiments with TopHat and cufflinks. *Nat Protoc* **7**: 562–578.
- Wong LH, McGhie JD, Sim M, Anderson MA, Ahn S, Hannan RD, George AJ, Morgan KA, Mann JR, Choo KH. 2010. ATRX interacts with H3.3 in maintaining telomere structural integrity in pluripotent embryonic stem cells. *Genome Res* **20**: 351–360.
- Wu J, Cui N, Wang R, Li J, Wong J. 2012. A role for CARM1-mediated histone H3 arginine methylation in protecting histone acetylation by releasing corepressors from chromatin. *PLoS One* **7**: e34692.
- Wu M, Wang L, Li Q, Li J, Qin J, Wong J. 2013. The MTA family proteins as novel histone H3 binding proteins. *Cell Biosci* **3**: 1.
- Xue Y, Wong J, Moreno GT, Young MK, Cote J, Wang W. 1998. NURD, a novel complex with both ATP-dependent chromatin-remodeling and histone deacetylase activities. *Mol Cell* **2**: 851–861.
- Yamada T, Yang Y, Hemberg M, Yoshida T, Cho HY, Murphy JP, Fioravante D, Regehr WG, Gygi SP, Georgopoulos K, et al. 2014. Promoter decompaction by the NuRD chromatin remodeling complex triggers synaptic connectivity in the mammalian brain. *Neuron* **83**: 122–134.
- Yang Y, Yamada T, Hill KK, Hemberg M, Reddy NC, Cho HY, Guthrie AN, Oldenborg A, Heiney SA, Ohmae S, et al. 2016. Chromatin remodeling inactivates activity genes and regulates neural coding. *Science* **353**: 300–305.
- Yildirim O, Li R, Hung JH, Chen PB, Dong X, Ee LS, Weng Z, Rando OJ, Fazio TG. 2011. Mbd3/NURD complex regulates expression of 5-hydroxymethylcytosine marked genes in embryonic stem cells. *Cell* **147**: 1498–1510.
- Zegerman P, Canas B, Pappin D, Kouzarides T. 2002. Histone H3 lysine 4 methylation disrupts binding of nucleosome remodeling and deacetylase (NuRD) repressor complex. *J Biol Chem* **277**: 11621–11624.
- Zhang Y, LeRoy G, Seelig HP, Lane WS, Reinberg D. 1998. The dermatomyositis-specific autoantigen Mi2 is a component of a complex containing histone deacetylase and nucleosome remodeling activities. *Cell* **95**: 279–289.
- Zhang Y, Liu T, Meyer CA, Eeckhoutte J, Johnson DS, Bernstein BE, Nusbaum C, Myers RM, Brown M, Li W, et al. 2008. Model-based Analysis of ChIP-Seq (MACS). *Genome Biol* **9**: R137.

Received February 20, 2018; accepted in revised form September 13, 2018.